JAERI-M
93-116

STUDIES OF WASTE FORM AND BUFFER MATERIAL PERFORMANCE AT JAPAN ATOMIC ENERGY RESEARCH INSTITUTE

June 1993

Tsunetaka BANBA, Hisayoshi MITAMURA
Naofumi KOZAI and Yaohiro INAGAKI*

日本原子力研究所
Japan Atomic Energy Research Institute

JAERI-Mレポートは，日本原子力研究所が不定期に公刊している研究報告書です。
入手の問合わせは，日本原子力研究所技術情報部情報資料課（〒319-11茨城県那珂郡東海村）あて，お申しこしください。なお，このほかに財団法人原子力弘済会資料センター（〒319-11 茨城県那珂郡東海村日本原子力研究所内）で複写による実費頒布をおこなっております。

JAERI-M reports are issued irregularly.
Inquiries about availability of the reports should be addressed to Information Division, Department of Technical Information, Japan Atomic Energy Research Institute, Tokai-mura, Naka-gun, Ibaraki-ken 319-11, Japan.

© Japan Atomic Energy Research Institute, 1993

編集兼発行　日本原子力研究所
印　　刷　㈱原子力資料サービス

JAERI-M 93-116

Studies of Waste Form and Buffer Material Performance at Japan Atomic Energy Research Institute

Tsunetaka BANBA, Hisayoshi MITAMURA, Naofumi KOZAI and Yaohiro INAGAKI*

Department of Environmental Safety Research
Tokai Research Establishment
Japan Atomic Energy Research Institute
Tokai-mura, Naka-gun, Ibaraki-ken

(Received April 27, 1993)

The recent studies of high-level radioactive waste forms and buffer material at Japan Atomic Energy Research Institute can be classified into the following three categories;

(1) Study on the radiation (alpha-radiation) effects which have relation to the microstructure of a nuclear waste glass.
(2) Study on the long-term self-irradiation damage of a SYNROC waste form using a curium-doped sample.
(3) Study on the sorption behavior of neptunium onto smectite which is one of major components of betonite.

In the present report, the recent results corresponding to the above categories are described.

Keywords: Nuclear Waste Glass, Alpha-decay, Helium Bubble, Synroc, Density, Leaching, Sorption, Smectite, Ion-exchange

---

This report was prepared for the Second Research Coordination Meeting of the IAEA Coordinated Research Program (CRP) on "Performance of High-Level Waste Forms and Packages under Repository Conditions", which was held in Bombay, India, from 5 to 9 April 1993.
* Kyushu University

JAERI-M 93-116

原研における高レベル放射性廃棄物固化体及び緩衝材に関する最近の研究成果

日本原子力研究所東海研究所環境安全研究部
馬場　恒孝・三田村久吉・香西　直文・稲垣八穂広*

(1993年4月27日受理)

原研における高レベル放射性廃棄物固化体及び緩衝材に関する最近の研究は，次の3つに大別できる。

(1) ガラス固化体の微細構造に及ぼす放射線照射の影響（特にα崩壊による影響）に関する研究。

(2) キュリウム添加試料を使用したシンロック固化体の放射線損傷に関する研究。

(3) 緩衝材候補としてのベントナイトの主成分の一つであるスメクタイトへのネプツニウムの収着挙動に関する研究。

本報告書では，それぞれに関係する最近の研究成果を報告する。

本報告書の内容は1993年4月，インドのボンベーで開催されたＩＡＥＡ協力研究計画（ＣＲＰ）「処分条件下の高レベル廃棄物固化体及び固化体容器の性能に関する研究調整会議」で発表したものをまとめたものである。

東海研究所：〒319-11　茨城県那珂郡東海村白方字白根2－4

＊　九州大学

Contents

目　　次

1. Introduction

The Japan Atomic Energy Research Institute (JAERI) has contributed to the establishment of the national system for the high-level radioactive waste management with developments of safety assessment methods and accumulation of useful data. Besides, JAERI is responsible for researches of new technology to be acceptable to the Japanese environmental circumstances.

In the present document, the JAERI's studies on the properties of the nuclear waste forms and buffer materials are described briefly.

2. Effects of Alpha-Decay on Microstructure of Simulated Nuclear Waste Glass [1]

The radiation effects on the properties of high-level waste glasses have been investigated using some irradiation techniques. Experimental data of radiation-induced changes in volume, stored energy and mechanical properties have been obtained by a number of investigators, but the mechanism of these changes has not been well understood. It has been generally assumed that most radiation-induced changes in the waste glass properties are related to damages from direct atomic displacements produced by elastic collisions and from electronic excitations resulting from ionization processes. In the waste glass, helium atoms are generated from alpha-decay of actinides and it is expected that helium bubbles are formed after exceeding its amount beyond the solubility limit in the waste glass[2]. The helium bubble formation has a great influence especially on volume and mechanical properties of the waste glass[3,4].

The purpose of this study is to investigate the microstructural changes of the irradiated waste glass. The microstructural changes of a simulated waste glass irradiated with doping of ^{238}Pu and ^{244}Cm were observed before and after annealing. On the basis of the results, the behavior of helium bubbles and its influence on the glass volume were discussed.

The composition of a simulated nuclear waste glass used is shown in Table I. The glass was self-irradiated from alpha-decay of doped ^{238}Pu and ^{244}Cm for about 7 years. The cumulative number of alpha-decays in the glass was 2.75×10^{25} alpha-decays/m^3. After irradiation, the glass was cut off to the size of 3-mm-diameter x 5.4-mm-height. The irradiated glasses were annealed in the air at 400°C for the period up to 6 hrs. Microstructures of the unirradiated, irradiated and irradiated/annealed samples were observed. A preshadowed carbon

1. Introduction

The Japan Atomic Energy Research Institute (JAERI) has contributed to the establishment of the national system for the high-level radioactive waste management with developments of safety assessment methods and accumulation of useful data. Besides, JAERI is responsible for researches of new technology to be acceptable to the Japanese environmental circumstances.

In the present document, the JAERI's studies on the properties of the nuclear waste forms and buffer materials are described briefly.

2. Effects of Alpha-Decay on Microstructure of Simulated Nuclear Waste Glass [1]

The radiation effects on the properties of high-level waste glasses have been investigated using some irradiation techniques. Experimental data of radiation-induced changes in volume, stored energy and mechanical properties have been obtained by a number of investigators, but the mechanism of these changes has not been well understood. It has been generally assumed that most radiation-induced changes in the waste glass properties are related to damages from direct atomic displacements produced by elastic collisions and from electronic excitations resulting from ionization processes. In the waste glass, helium atoms are generated from alpha-decay of actinides and it is expected that helium bubbles are formed after exceeding its amount beyond the solubility limit in the waste glass[2]. The helium bubble formation has a great influence especially on volume and mechanical properties of the waste glass[3,4].

The purpose of this study is to investigate the microstructural changes of the irradiated waste glass. The microstructural changes of a simulated waste glass irradiated with doping of ^{238}Pu and ^{244}Cm were observed before and after annealing. On the basis of the results, the behavior of helium bubbles and its influence on the glass volume were discussed.

The composition of a simulated nuclear waste glass used is shown in Table I. The glass was self-irradiated from alpha-decay of doped ^{238}Pu and ^{244}Cm for about 7 years. The cumulative number of alpha-decays in the glass was 2.75×10^{25} alpha-decays/m^3. After irradiation, the glass was cut off to the size of 3-mm-diameter x 5.4-mm-height. The irradiated glasses were annealed in the air at 400°C for the period up to 6 hrs. Microstructures of the unirradiated, irradiated and irradiated/annealed samples were observed. A preshadowed carbon

replica technique in combination with scanning electron microscopy (SEM) was used for the observation.

Fig.1(A) and (B) show the fracture surfaces of unirradiated and irradiated glass. About 200 bubbles in a few tens of micrographs were investigated to measure the bubble radius and bubble density and the averages of them were calculated to be 0.23 μm and $1x10^{17}$ bubbles/m^3, respectively. The fractured surfaces of the glass annealed at 400°C for 3 hrs after irradiation are shown in Fig.1(C), in which bubbles with the average radius of 0.12 μm were observed. The average bubble radius during annealing at 400°C as a function of annealing time is shown in Fig.2 as open circles. The bubble radius was observed to decrease with annealing time.

The bubble behavior during annealing was analyzed on the basis of the helium diffusion model with two chemical processes, i.e. trapping at bubbles and re-solution from bubbles into glass matrix[5,6]. In this model helium atoms in the glass were analyzed with the situation when diffusion occurs in a medium containing a stable array of trapping sites (He bubbles). Schematic representative of the situation is shown in Fig.3. Diffusion equation of this process in a cylindrical glass specimen is described by

$$\partial C/\partial t = D\{\partial^2 C/\partial r^2 + (1/r)(\partial C/\partial r) + \partial^2 C/\partial z^2\} - gC + bM, \qquad (1)$$

where C is the concentration of helium in glass matrix, M is the number of helium atoms trapped in bubbles per unit glass volume, t is the annealing time, g is the trapping rate constant per unit time, b is the re-solution rate constant per unit time, r and z are radial and vertical positions in a specimen. The balance for the trapped helium is given by

$$\partial M/\partial t = gC - bM, \qquad (2)$$

For simplicity, the average of M(r,z,t) is given by

$$M(t) = (8/\pi a^2 LC_B) \int_0^{\pi/2}\int_0^{L/2}\int_0^{a} M(r,z,t)\, dr\, dz\, d\theta, \qquad (3)$$

where a and L represent a radius and a height of the glass specimen, and C_B is the bubble density. Eqs.(1) and (2) were solved by a numerical method under the initial and boundary conditions determined by experimental conditions[1], and the number of helium atoms in bubbles per unit glass volume as a function of annealing time, M(t), was obtained.

The situation of a helium bubble embedded in the glass matrix is shown in Fig.4 and the equilibrium condition for a helium bubble of radius R is

$$R = 2\gamma / p, \tag{4}$$

where γ and p represent the surface tension of the glass and the helium pressure in a bubble, respectively. Supposing ideal gas behavior, the number of helium atoms in a bubble at annealing time t, m(t), is related to the bubble radius by

$$m(t) = 8\pi\gamma R(t)^2 / (3k_B T) , \tag{5}$$

where k_B is Boltzmann's constant and T is the temperature(K). Assuming that the bubble density C_B during annealing is constant and all trap site makes a bubble with uniform size, the bubble radius is described as a function of M(t),

$$R(t) = \{3k_B T m(t) / (8\pi\gamma)\}^{0.5} = \{3k_B T M(t) / (8\pi\gamma C_B)\}^{0.5} \tag{6}$$

Using Eq.(6) the bubble radius,R(t), was calculated.

The values of D, g and b shown in Table II, which had been obtained experimentally in our previous study on helium release[7], were applied to the calculation of R(t). Because the value of is unknown, the following relation[8] was applied for all temperature,

$$2\gamma / (k_B T) = 1.0 \times 10^{20} \ [m^{-2}] . \tag{7}$$

The calculated curve of R(t) at 400°C is shown in Fig.2 as a solid line. The agreement between the calculated and observed bubble radius was relatively good.

In our previous study[9] the irradiated (1.7×10^{25} alpha-decays/m^3) glass had been annealed and the volume change as a function of annealing time had been measured. The measured volume change at 400°C as a function of annealing time is shown in Fig.5 as open circles. Supposing that the volume change of glass results from bubble formation, the following equation is obtained:

$$\Delta V / V_0 \cong 4\pi R^3 C_B / 3 \tag{8}$$

where V_0 is the original glass volume and ΔV is the volume increase due to helium bubbles. Assuming that the bubble density is constant during annealing and the bubble size in the glass is uniform, the volume change as a function of annealing time was calculated from Eqs.(6) and (8).

The calculated curve is shown in Fig.5 as a solid line. The calculated curve was in good agreement with the measured volume change, which suggests that the volume change during annealing is controlled mainly by the behavior of helium bubbles.

3. Aging Effects on Curium-Doped Synroc Containing Sodium-Bearing High-Level Nuclear Waste [10]

In a previous study[11], densities and leaching behavior of the curium-doped titanate ceramic containing sodium-bearing HLW (see the nominal composition of sample shown in Table III), which had accumulated a dose up to ~7 x 10^{17} alpha-decays/g were examined. Although samples up to a dose of 2.8 x 10^{17} alpha-decays/g, corresponding to an equivalent age of 330 yr, showed a volume swelling of 0.4 %, their chemical durability was not measurably affected. Some samples that had accumulated a dose of 5.6 x 10^{17} alpha-decays/g (equivalent age, 2000 yr), however, showed significant deterioration of their chemical durability.

In the present work, the curium-doped samples, having now sustained much more damage, were subjected to optical observation, density measurement and leach testing to clarify further self-irradiation effects. The density of samples was measured by the water displacement method. Half-disk specimens of 2 cm in diameter and 0.1-0.2 cm in thickness were MCC-1 leach tested in distilled water at 90°C for two months over four 7-day and a 28-day leach periods[11].

A gradual decrease in density, which was fitted by a line, continued up to a dose of 8.5 x 10^{17} alpha-decays/g (equivalent age, 9000 yr). After that, the rate of density change increased and approached a constant value (Fig.6). The extrapolated density reduction based on the linear relationship would be -2.2% after a dose of 15.7 x 10^{17} alpha-decays/g (equivalent age, 10^5 yr), while the measured value reached -3.4% at the same age. This discrepancy may be due to crack propagation. Figure 7 shows optical micrographs of the sample at doses of 7.9 x and 12.5 x 10^{17} alpha-decays/g, which correspond to equivalent ages of 7300 and 33000 yr, respectively. For the smaller dose, a few cracks, 1 μm wide and 0.1 to 0.5 mm in length, are arrowed in Fig. 7(a). At the higher dose (Fig. 7(b)), the cracks were larger and prolific with a maximum length and width of 2.9 mm and 10 μm, respectively.

Figure 8 and 9 show the variation in leachate pH and the normalized leach rates of nonradioactive elements with time; data from the 130-yr samples are included as a reference[11]. As seen in Fig.8, the 11000-

The calculated curve is shown in Fig.5 as a solid line. The calculated curve was in good agreement with the measured volume change, which suggests that the volume change during annealing is controlled mainly by the behavior of helium bubbles.

3. Aging Effects on Curium-Doped Synroc Containing Sodium-Bearing High-Level Nuclear Waste [10]

In a previous study[11], densities and leaching behavior of the curium-doped titanate ceramic containing sodium-bearing HLW (see the nominal composition of sample shown in Table III), which had accumulated a dose up to ~7 x 10^{17} alpha-decays/g were examined. Although samples up to a dose of 2.8 x 10^{17} alpha-decays/g, corresponding to an equivalent age of 330 yr, showed a volume swelling of 0.4 %, their chemical durability was not measurably affected. Some samples that had accumulated a dose of 5.6 x 10^{17} alpha-decays/g (equivalent age, 2000 yr), however, showed significant deterioration of their chemical durability.

In the present work, the curium-doped samples, having now sustained much more damage, were subjected to optical observation, density measurement and leach testing to clarify further self-irradiation effects. The density of samples was measured by the water displacement method. Half-disk specimens of 2 cm in diameter and 0.1-0.2 cm in thickness were MCC-1 leach tested in distilled water at 90°C for two months over four 7-day and a 28-day leach periods[11].

A gradual decrease in density, which was fitted by a line, continued up to a dose of 8.5 x 10^{17} alpha-decays/g (equivalent age, 9000 yr). After that, the rate of density change increased and approached a constant value (Fig.6). The extrapolated density reduction based on the linear relationship would be -2.2% after a dose of 15.7 x 10^{17} alpha-decays/g (equivalent age, 10^5 yr), while the measured value reached -3.4% at the same age. This discrepancy may be due to crack propagation. Figure 7 shows optical micrographs of the sample at doses of 7.9 x and 12.5 x 10^{17} alpha-decays/g, which correspond to equivalent ages of 7300 and 33000 yr, respectively. For the smaller dose, a few cracks, 1 μm wide and 0.1 to 0.5 mm in length, are arrowed in Fig. 7(a). At the higher dose (Fig. 7(b)), the cracks were larger and prolific with a maximum length and width of 2.9 mm and 10 μm, respectively.

Figure 8 and 9 show the variation in leachate pH and the normalized leach rates of nonradioactive elements with time; data from the 130-yr samples are included as a reference[11]. As seen in Fig.8, the 11000-

yr samples display an average pH in the specimen-charged leachates which is always higher than that of the specimen-free leachate; the average final pH reaches 8.4. The initial leach period for the 31000-yr samples gives the high average pH value of 9.3 in the specimen-charged leachates. For longer leach times, the average pH of the specimen-charged leachates decreases quickly.

Leach data from the 130-yr samples indicate the following order of leach rates:

Na ~ Mo > Cs > Sr ~ Ca.

Although the scatter within the triplicates is large, a factor of four at maximum, the leach rates of elements from the 11000-yr samples are nearly constant with leach time, and much higher than those from the 130-yr samples. The leach rates from the 11000-yr samples decrease as follows:

Na ~ Cs > Mo > Sr > Ca > Ba.

Dissolution of elements from the 31000-yr samples shows similar time dependence to the 130-yr samples even though the former samples give markedly higher leach rates. After the initial leach period, the leach rate of cesium decreases with time in the same manner as that of barium, but always remains slightly higher. For the 31000-yr samples, the orders of the leach rates are:

Na ~ Cs > Sr > Ca ~ Mo > Ba (initial leach period),

Sr ~ Ca ~ Na ~ Mo > Cs > Ba (final leach period).

There is a direct correlation between pH and the release of the nonradioactive elements, particularly the alkalis. For the 11000-yr samples, the final pH of the specimen-charged leachates was much higher than the preceding leach periods, although the leach rates of the elements were nearly constant. A contributing factor is that the final leach period was four times longer than the preceding leach periods.

To aid data analysis, the constituents of the polyphase assemblage were classified into two groups: the actinide-host phases (perovskite and zirconolite phases) rich in strontium and calcium, and actinide-free phases (freudenbergite, hollandite, metallic and intergranular phases) rich in sodium, cesium, barium and molybdenum. In leach testing on the 130-yr samples (1.9×10^{17} alpha-decays/g), the freudenbergite and hollandite phases controlled the release of sodium, and cesium and barium, respectively, while the perovskite and/or freudenbergite phases controlled strontium and calcium losses. It is also possible that intergranular phases affected the release of the alkalis. It was argued that volume swelling, resulting from the accumulation of alpha-decay damage, exposed fresh surfaces in the 11000- and 31000-yr samples ($9.1 \times$ and 12.3×10^{17} alpha-decays/g, respectively), with intergranular phases dominating the leaching of sodium and cesium and significantly affecting that of strontium. This suggests that the high contents of

the processing contaminants (particularly sodium) promoted enrichment of strontium at intergranular phases[12].

The diminution of chemical durability of the crystalline phases as a function of damage ingrowth was apparent by comparison of the leach rates of the indicator elements in the 130- and 31000-yr samples as shown in Fig.10. The leach rates of sodium and cesium in the latter case were ~10 times greater. Since these elements were contained within actinide-free phases, this 1-order-of-magnitude increase in the leach rates was deduced to arise mainly from the increase in effective surface areas due to crack propagation, with some minor contribution of alkali migration due to radiation effects[13]. On the other hand, the leach rates of strontium and calcium increased more than those of sodium and cesium by 1 order of magnitude (i.e. a factor of $\sim 10^2$ as a total). This additional increase appears to be the result of deterioration of the actinide-host phases due to alpha-recoil damage. The deterioration of the actinide-host phases could not be monitored by curium dissolution because this was pH and Eh limited, rather than being controlled by structural breakdown. While the accumulation of alpha-decay damage in the titanate ceramic waste form leads to an increase in the leach rates of cesium and strontium, it is noted that this occurs at a damage level at which the cesium-137 and strontium-90 decay to harmless levels in the waste form.

4. Sorption Characteristics of Neptunium onto Sodium-Smectite[14]

Since bentonite is a candidate backfill material for nuclear waste isolation, it is necessary to clarify the sorption mechanisms of long-lived actinides onto bentonite for the safety evaluation on the waste isolation. Bentonite is a mixture of different minerals such as smectite, quartz, pyrite and calcite and its properties are very complicated. In the present work, the sorption behaviors of neptunium onto smectite, which is one of major components of bentonite, are investigated.

The chemical composition of the smectite, which consists mainly of dioctahedral smectite (montmorillonite), is shown in Table IV. This smectite is changed to sodium-type smectite by using a 5M-NaCl solution. The Na-smectite powder of 0.06 g is contacted with 6 ml 0.01M-$NaClO_4$ solution containing 6×10^{-7} mol/l of ^{237}Np in a polycarbonate tube for 10 days at 20°C. The pH of neptunium solution is adjusted with HCl and NaOH solutions. The pH and ^{237}Np concentration of the supernatant after centrifuging for 1 hr at 12000 rpm are measured by a pH meter and a liquid scintillation counter, respectively. The smectite which have sorbed ^{237}Np are immersed in a desorbing 1M-KCl solution for 2 days at

the processing contaminants (particularly sodium) promoted enrichment of strontium at intergranular phases[12].

The diminution of chemical durability of the crystalline phases as a function of damage ingrowth was apparent by comparison of the leach rates of the indicator elements in the 130- and 31000-yr samples as shown in Fig.10. The leach rates of sodium and cesium in the latter case were ~10 times greater. Since these elements were contained within actinide-free phases, this 1-order-of-magnitude increase in the leach rates was deduced to arise mainly from the increase in effective surface areas due to crack propagation, with some minor contribution of alkali migration due to radiation effects[13]. On the other hand, the leach rates of strontium and calcium increased more than those of sodium and cesium by 1 order of magnitude (i.e. a factor of $\sim 10^2$ as a total). This additional increase appears to be the result of deterioration of the actinide-host phases due to alpha-recoil damage. The deterioration of the actinide-host phases could not be monitored by curium dissolution because this was pH and Eh limited, rather than being controlled by structural breakdown. While the accumulation of alpha-decay damage in the titanate ceramic waste form leads to an increase in the leach rates of cesium and strontium, it is noted that this occurs at a damage level at which the cesium-137 and strontium-90 decay to harmless levels in the waste form.

4. Sorption Characteristics of Neptunium onto Sodium-Smectite[14]

Since bentonite is a candidate backfill material for nuclear waste isolation, it is necessary to clarify the sorption mechanisms of long-lived actinides onto bentonite for the safety evaluation on the waste isolation. Bentonite is a mixture of different minerals such as smectite, quartz, pyrite and calcite and its properties are very complicated. In the present work, the sorption behaviors of neptunium onto smectite, which is one of major components of bentonite, are investigated.

The chemical composition of the smectite, which consists mainly of dioctahedral smectite (montmorillonite), is shown in Table IV. This smectite is changed to sodium-type smectite by using a 5M-NaCl solution. The Na-smectite powder of 0.06 g is contacted with 6 ml 0.01M-$NaClO_4$ solution containing 6×10^{-7} mol/l of ^{237}Np in a polycarbonate tube for 10 days at 20°C. The pH of neptunium solution is adjusted with HCl and NaOH solutions. The pH and ^{237}Np concentration of the supernatant after centrifuging for 1 hr at 12000 rpm are measured by a pH meter and a liquid scintillation counter, respectively. The smectite which have sorbed ^{237}Np are immersed in a desorbing 1M-KCl solution for 2 days at

20°C, and then in a 1M-HCl solution under the same condition. Both the solutions are used for desorbing the ion-exchangeable parts of neptunium ions sorbed on smectite (KCl)[15], and for desorbing the remaining neptunium sorbed strongly (HCl)[16]. The ^{237}Np activities of both the desorbing solutions are measured with a liquid scintillation counter. No residual ^{237}Np in the smectite samples was found by measuring the acidic decomposition solutions of smectites.

The pH dependence of the distribution coefficient (Kd) of ^{237}Np on the smectite is shown in Fig.11. The highest Kd (~$3x10^3$ ml/g) at pH 2.5 decreases with increasing pH, and Kds stabilize at ~20 ml/g between pH 5 and 8. Figure 12 shows the pH dependence of ^{237}Np fraction (%) desorbed by KCl and HCl solutions. Above pH 5, most of ^{237}Np sorbed on smectite was desorbed by KCl solution (Type A sorption). Below pH 5, the fraction of ^{237}Np desorbed by HCl solution (Type B sorption) increases with decreasing pH of sorbing solution.

These results suggest that the neptunium is sorbed onto smectite by two different mechanisms: "Type A sorption", which is controlled by the ion-exchange mechanism ($R\text{-}Na + NpO_2^+(aq) \rightleftharpoons R\text{-}NpO_2 + Na^+$; the dominant species of neptunium in solution at pH 2-8 is considered to be $NpO_2^+(aq)$[17]), and "Type B sorption", which is correlated to the structure of smectite.

The neptunium can not have access to the interlayer of smectite in neutral pH (5-8) solution, because the interlayer spacing of smectite may be smaller than the radius of the neptunium aqueous ion ($NpO_2^+(aq)$). In this pH region, therefore, most of the neptunium is sorbed on the outer surface of smectite by the ion-exchange mechanism (Type A sorption). This is supported by the fact that the Kd of neptunium is smaller by two order of magnitude than those of Sr^{2+} and Cs^+ which have access to both the outer surface and the interlayer[18].

Figure 13 shows the X-ray diffraction (XRD) patterns indicating the structure change of smectite by the contact with the pH 2.5 solution. The XRD patterns in this figure were taken from (a) the Na-smectite used for the sorption experiments, (b) smectite treated with pH 2.5 solution, (c) smectite treated with pH 7.4 solution and (d) smectite treated with pH 10.9, respectively. The peak at 2θ =~7° on the XRD pattern from Na-smectite shifted to ~6.5° by only contacting the acidic solution. This change implies that the basal spacing of Na-smectite was expanded from 1.25 nm to 1.48 nm after soaking Na-smectite in the pH 2.5 solution. Since the basal spacing of collapsed smectite is approximately 0.95 nm[19], the interlayer spacing of smectite soaked in the acidic solution is estimated to be larger by a factor of 1.8 than that of Na-smectite. In the low pH (<5) solutions, therefore, the neptunium aqueous ion probably have access to the interlayer expanded by exchanging the

interlayer cation of H^+ with Na^+ (Type B sorption). Consequently, the neptunium is sorbed at both the outer surface and the interlayer of smectite. This is closely linked to the increase in the Kd of neptunium in the low pH solution, and the Kd of neptunium has the same order as those of Sr^{2+} and Cs^+ [18].

5. Future Work

At JAERI the safety evaluation studies of waste forms and engineered barrier materials are in progress along the following three items.

1. Leaching behaviors of actinide-doped waste glasses under repository conditions will be investigated for the clarification of actinide release mechanisms.
2. The capability and feasibility will be evaluated for titanate or zirconia based ceramic forms for the high-level radioactive waste.
3. Sorption and desorption behaviors of actinides on backfill and overpack materials will be investigated under repository conditions for the long-term assessment of nuclear waste disposal.

In addition, the radioactive glass characterization program is in progress with the object of corroborating the information provided on the data sheet attached to the vitrified waste containers, with the results of tests and measurements performed on samples of industrial vitrified products (COGEMA and BNFL).

Acknowledgment

The authors wish to thank Dr. S.Muraoka for helpful suggestions and a critical reading of the manuscript.

References

[1] INAGAKI, Y. et al., Mat. Res. Soc. Symp. Proc., Vol.257 (1992) 199.
[2] SATO,S. et al., J. Nucl. Mater., **152** (1988) 489.
[3] WEBER, W.J., Nucl. Instr. and Meth., **B32** (1988) 471.
[4] WEBER, W.J., Matzke, H., PNL-SA-13907 (1986).
[5] OLANDER, D.R., Fundamental Aspects of Nuclear Reactor Fuel Elements, ERDA, Springfield, Virginia (1976) 307.
[6] TURCOTTE, R.P., BNWL-2051 (1976).
[7] MORIKAWA, K. et al., J. Nucl. Sci. Technol., to be published.
[8] WEBER, W.J., ROBERTS, F.P., Nucl. Technol., **60** (1983) 178.

interlayer cation of H^+ with Na^+ (Type B sorption). Consequently, the neptunium is sorbed at both the outer surface and the interlayer of smectite. This is closely linked to the increase in the Kd of neptunium in the low pH solution, and the Kd of neptunium has the same order as those of Sr^{2+} and Cs^+ [18].

5. Future Work

At JAERI the safety evaluation studies of waste forms and engineered barrier materials are in progress along the following three items.

1. Leaching behaviors of actinide-doped waste glasses under repository conditions will be investigated for the clarification of actinide release mechanisms.
2. The capability and feasibility will be evaluated for titanate or zirconia based ceramic forms for the high-level radioactive waste.
3. Sorption and desorption behaviors of actinides on backfill and overpack materials will be investigated under repository conditions for the long-term assessment of nuclear waste disposal.

In addition, the radioactive glass characterization program is in progress with the object of corroborating the information provided on the data sheet attached to the vitrified waste containers, with the results of tests and measurements performed on samples of industrial vitrified products (COGEMA and BNFL).

Acknowledgment

The authors wish to thank Dr. S.Muraoka for helpful suggestions and a critical reading of the manuscript.

References

[1] INAGAKI, Y. et al., Mat. Res. Soc. Symp. Proc., Vol.257 (1992) 199.
[2] SATO,S. et al., J. Nucl. Mater., **152** (1988) 489.
[3] WEBER, W.J., Nucl. Instr. and Meth., **B32** (1988) 471.
[4] WEBER, W.J., Matzke, H., PNL-SA-13907 (1986).
[5] OLANDER, D.R., Fundamental Aspects of Nuclear Reactor Fuel Elements, ERDA, Springfield, Virginia (1976) 307.
[6] TURCOTTE, R.P., BNWL-2051 (1976).
[7] MORIKAWA, K. et al., J. Nucl. Sci. Technol., to be published.
[8] WEBER, W.J., ROBERTS, F.P., Nucl. Technol., **60** (1983) 178.

interlayer cation of H^+ with Na^+ (Type B sorption). Consequently, the neptunium is sorbed at both the outer surface and the interlayer of smectite. This is closely linked to the increase in the Kd of neptunium in the low pH solution, and the Kd of neptunium has the same order as those of Sr^{2+} and Cs^+ [18].

5. Future Work

At JAERI the safety evaluation studies of waste forms and engineered barrier materials are in progress along the following three items.

1. Leaching behaviors of actinide-doped waste glasses under repository conditions will be investigated for the clarification of actinide release mechanisms.
2. The capability and feasibility will be evaluated for titanate or zirconia based ceramic forms for the high-level radioactive waste.
3. Sorption and desorption behaviors of actinides on backfill and overpack materials will be investigated under repository conditions for the long-term assessment of nuclear waste disposal.

In addition, the radioactive glass characterization program is in progress with the object of corroborating the information provided on the data sheet attached to the vitrified waste containers, with the results of tests and measurements performed on samples of industrial vitrified products (COGEMA and BNFL).

Acknowledgment

The authors wish to thank Dr. S.Muraoka for helpful suggestions and a critical reading of the manuscript.

References

[1] INAGAKI, Y. et al., Mat. Res. Soc. Symp. Proc., Vol.257 (1992) 199.
[2] SATO,S. et al., J. Nucl. Mater., **152** (1988) 489.
[3] WEBER, W.J., Nucl. Instr. and Meth., **B32** (1988) 471.
[4] WEBER, W.J., Matzke, H., PNL-SA-13907 (1986).
[5] OLANDER, D.R., Fundamental Aspects of Nuclear Reactor Fuel Elements, ERDA, Springfield, Virginia (1976) 307.
[6] TURCOTTE, R.P., BNWL-2051 (1976).
[7] MORIKAWA, K. et al., J. Nucl. Sci. Technol., to be published.
[8] WEBER, W.J., ROBERTS, F.P., Nucl. Technol., **60** (1983) 178.

interlayer cation of H^+ with Na^+ (Type B sorption). Consequently, the neptunium is sorbed at both the outer surface and the interlayer of smectite. This is closely linked to the increase in the Kd of neptunium in the low pH solution, and the Kd of neptunium has the same order as those of Sr^{2+} and Cs^+ [18].

5. Future Work

At JAERI the safety evaluation studies of waste forms and engineered barrier materials are in progress along the following three items.

1. Leaching behaviors of actinide-doped waste glasses under repository conditions will be investigated for the clarification of actinide release mechanisms.
2. The capability and feasibility will be evaluated for titanate or zirconia based ceramic forms for the high-level radioactive waste.
3. Sorption and desorption behaviors of actinides on backfill and overpack materials will be investigated under repository conditions for the long-term assessment of nuclear waste disposal.

In addition, the radioactive glass characterization program is in progress with the object of corroborating the information provided on the data sheet attached to the vitrified waste containers, with the results of tests and measurements performed on samples of industrial vitrified products (COGEMA and BNFL).

Acknowledgment

The authors wish to thank Dr. S.Muraoka for helpful suggestions and a critical reading of the manuscript.

References

[1] INAGAKI, Y. et al., Mat. Res. Soc. Symp. Proc., Vol.257 (1992) 199.
[2] SATO,S. et al., J. Nucl. Mater., **152** (1988) 489.
[3] WEBER, W.J., Nucl. Instr. and Meth., **B32** (1988) 471.
[4] WEBER, W.J., Matzke, H., PNL-SA-13907 (1986).
[5] OLANDER, D.R., Fundamental Aspects of Nuclear Reactor Fuel Elements, ERDA, Springfield, Virginia (1976) 307.
[6] TURCOTTE, R.P., BNWL-2051 (1976).
[7] MORIKAWA, K. et al., J. Nucl. Sci. Technol., to be published.
[8] WEBER, W.J., ROBERTS, F.P., Nucl. Technol., **60** (1983) 178.

[9] INAGAKI, Y., BANBA, T. et al., JAERI-M 90-225 (1990).
[10] MITAMURA, H. et al., J. Am. Ceram. Soc., **75** 2 (1992) 392.
[11] MITAMURA, H. et al., J. Am. Ceram. Soc., **73** 11 (1990) 3433.
[12] LEVIN, E.M., ROBBINS, C.R., McMURDIE, H.F., "Phase Diagrams for Ceramists," RESER, M. K., Ed., American Ceramic Society, Columbus, OH; Figs. 193 and 194 (1964).
[13] BURSILL, L.A., SMITH, D.J., J. Solid State Chem., **69** (1987) 343.
[14] KOZAI, N. et al., J. Nucl. Sci. Technol., to be published.
[15] JACKSON, R.E., INCH, K.J., Environ. Sci. Technol., **17** (1983) 231.
[16] BANERJEE, D.K. et al., Soil Sci., **75** (1953) 421.
[17] INOUE, Y., TOCHIYAMA, O., Technology Reports, Vol.47, Tohoku Univ., Sendai, Japan (1982) 263.
[18] MAES, A. et al., Clays and Clay Minerals, **33** (1985) 251.
[19] GREENLAND, D.J., HAYES, M.H.B. (Eds), The Chemistry of Soil Constituents, John Wiley & Sons Ltd. (1985) p.92.

Table I. Composition of a Simulated Waste Glass.

Component	wt %				
Additives		MnO_2	0.26	SeO_2	0.02
SiO_2	45.15	Ag_2O	0.03	RuO_2	0.80
B_2O_3	13.90	CdO	0.03	Fe_2O_3	2.90
Al_2C_3	4.89	SnO_2	0.02	NiO	0.40
Li_2O	2.00	Sb_2O_3	0.01	Cr_2O_3	0.50
Na_2O	9.78	TeO_2	0.23	P_2O_5	0.30
CaO	4.00	Cs_2O	0.97	Ru	0.12
ZnO	2.47	BaO	0.62	Rh	0.15
		La_2O_3	0.14	Pd	0.43
Wastes		CeO_2	0.28	Cm Oxides	3.04
Rb_2O	0.12	Pr_6O_{11}	0.14	Pu Oxides	0.96
SrO	0.34	Nd_2O_3	0.45		
Y_2O_3	0.06	Sm_3O_3	0.09	Total	100.00
ZrO_2	2.64	Eu_2O_3	0.02		
MoO_3	1.73	Gd_2O_3	0.01		

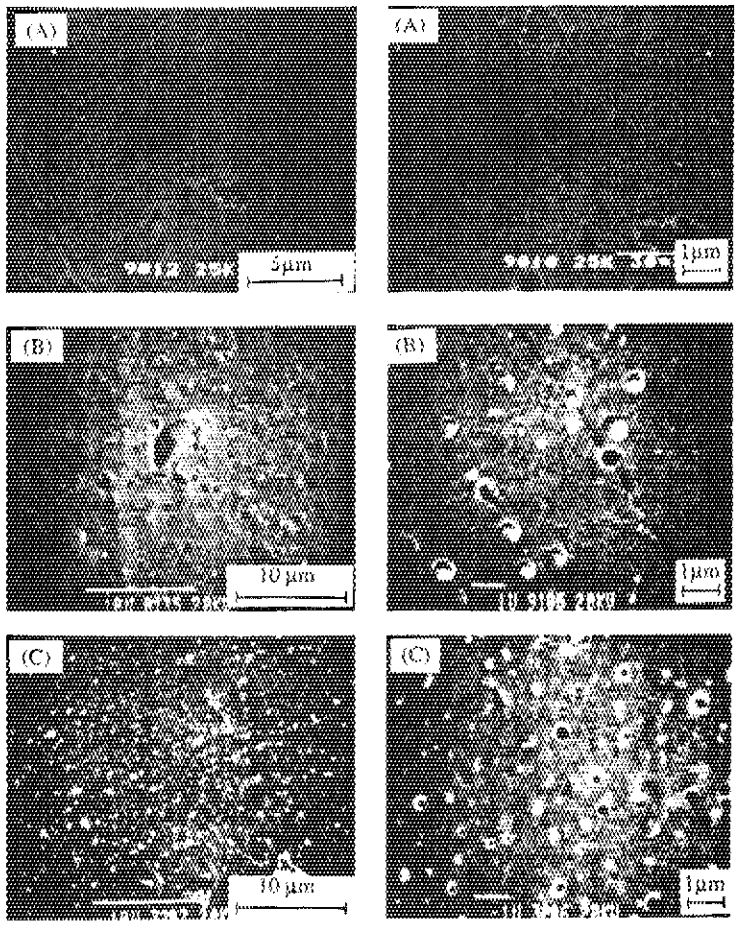

Fig.1. SEM micrographs of fractured surfaces for the simulated waste glass. (A) Unirradiated glass. (B) Glass irradiated at a dose of 2.75 x 10^{25} α-decay/m^3. (C) Glass annealed at 673K for 3 hours after irradiation.

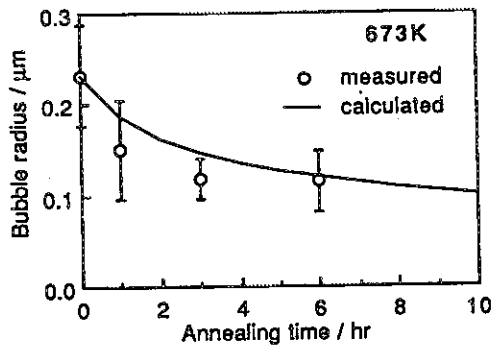

Fig.2. The average bubble radius during annealing at 673K as a function of annealing time.

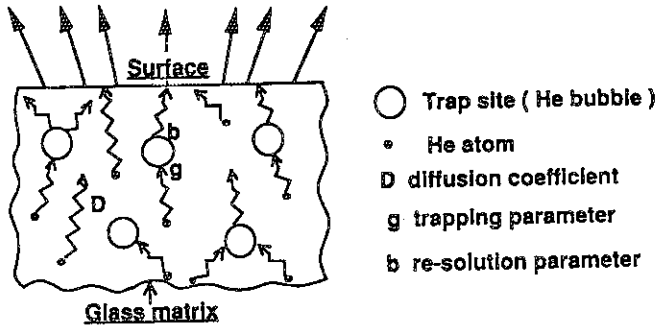

Fig.3. Schematic representative of helium diffusion model.

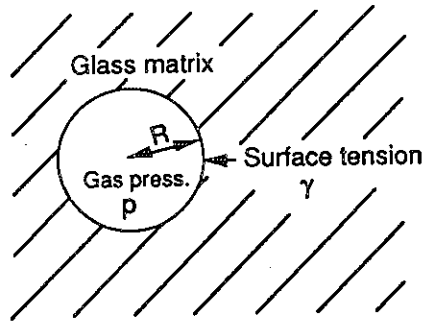

Fig.4. Helium bubble embedded in the glass matrix.

Table II. Values of parameters obtained in the previous study on helium release from the glass irradiated at a dose of 1.7×10^{25} α-decay/m^3[9].

$D = 2.0 \times 10^{-7} \exp(-12.7 \text{ kcal/RT})$ [m^2/sec]
$b = 1.1 \times 10^{5} \exp(-15.7 \text{ kcal/RT})$ [sec^{-1}]
$g = 0.1$ [sec^{-1}]

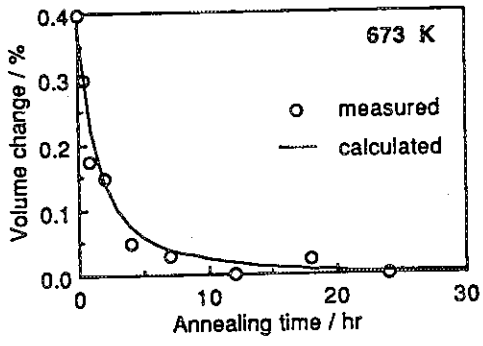

Fig.5. Volume change of the glass during postirradiation annealing at 673K.

Table III. Nominal Composition of Curium-Doped Titanate Ceramic

Element	Content (wt%)
Precursor	
TiO_2	62.24
CaO	9.70
ZrO_2	5.95
BaO	4.81
Al_2O_3	4.72
Oxygen getter	
Ti (metal)	1.99
Simulated HLW	
SeO_2	0.011
Rb_2O	0.064
SrO	0.176
Y_2O_3	0.104
ZrO_2	0.852
MoO_3	0.899
MnO_2	0.133
RuO_2	0.506
Rh_2O_3	0.105
PdO	0.276
Ag_2O	0.015
CdO	0.016
SnO_2	0.010
Sb_2O_3	0.002
TeO_2	0.118
Cs_2O	0.507
BaO	0.325
La_2O_3	0.263
CeO_2	0.524
Pr_6O_{11}	0.257
Nd_2O_3	0.237
$CmO_2 + PuO_2$	1.614
Na_2O	1.652
P_2O_5	0.167
Fe_2O_3	1.382
Cr_2O_3	0.200
NiO	0.175

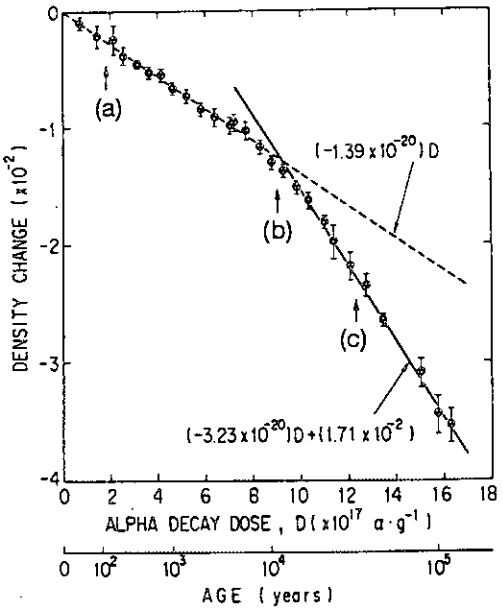

Fig. 6. Change in density of curium-doped block sample vs α-decay dose. Equivalent age corresponding to an α-decay dose (after Fig. 1 in Ref. 16) is also shown. Broken and solid lines indicate Eqs. (1) and (2), respectively. Arrows (a), (b), and (c) indicate increment in density at equivalent ages of 130, 11 000, and 31 000 yr, respectively.

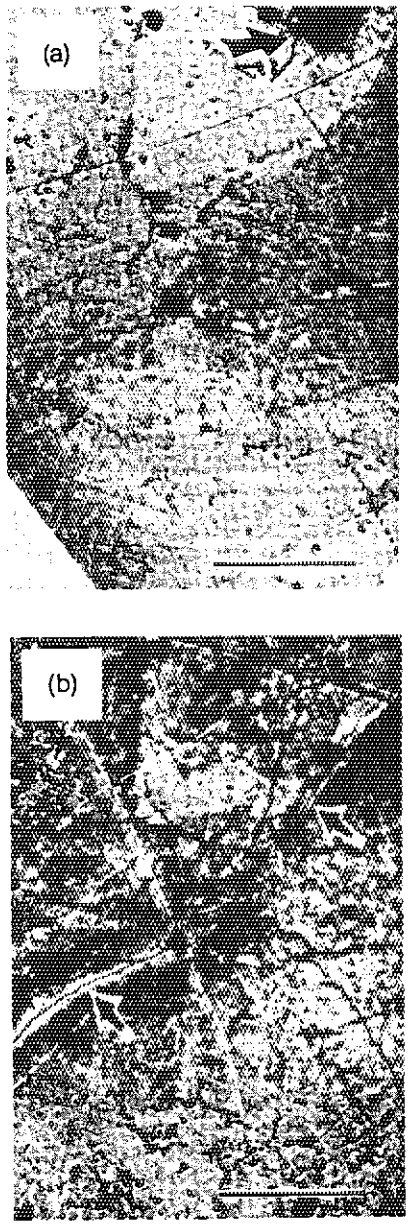

Fig. 7. Optical micrographs of block sample of curium-doped titanate ceramic at doses of (a) 7.9×10^{17} and (b) 12.5×10^{17} α decays·g^{-1}. Arrows indicate cracks. Scale bars = 0.5 mm.

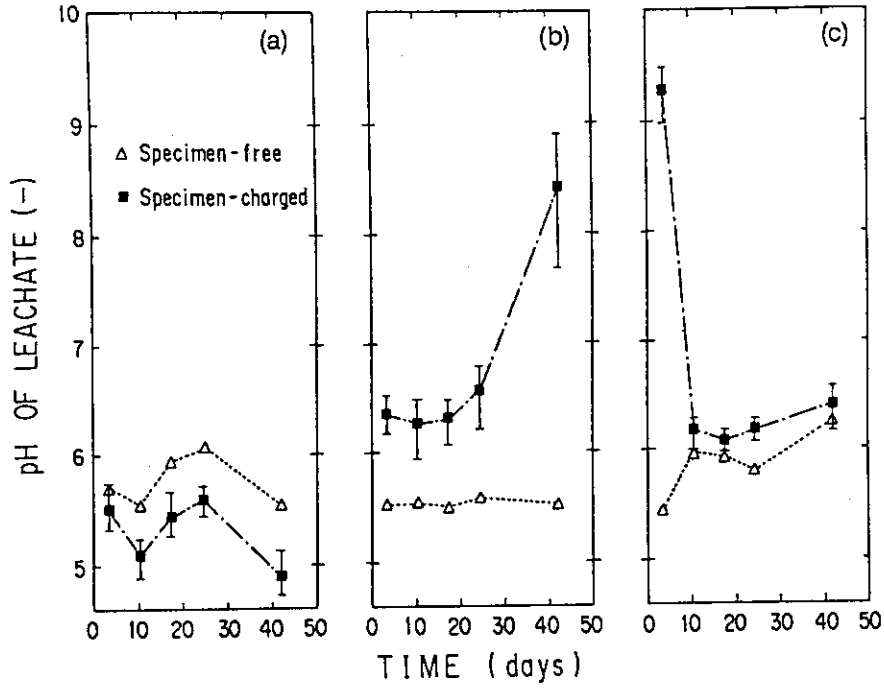

Fig. 8 Change in pH of leachate from curium-doped titanate ceramic vs leach time. (a), (b), and (c) correspond to equivalent ages of 130, 11000, and 31000 yr, respectively. Error bars attached to the average indicate the largest and smallest values among three sets of specimen-charged data in each run. In (a) and (c), displacement of specimen-free data in time is probably due to pH calibration problem.

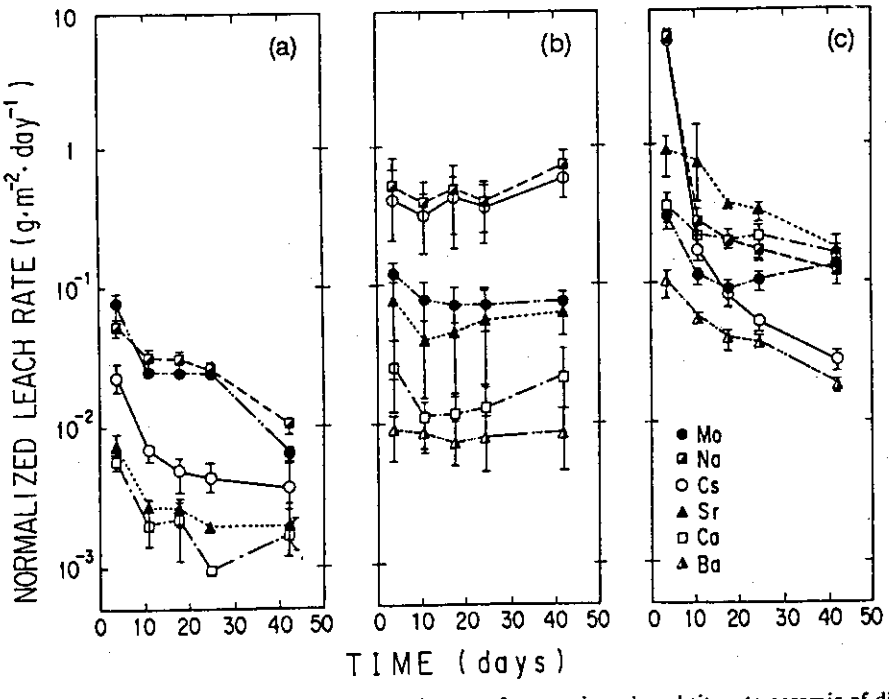

Fig. 9. Comparison of normalized leach rates of nonradioactive elements from curium-doped titanate ceramic of different ages. (a), (b), and (c) correspond to equivalent ages of 130, 11000, and 31000 yr, respectively. Error bars attached to the average indicate the largest and smallest values among three sets of data in each run.

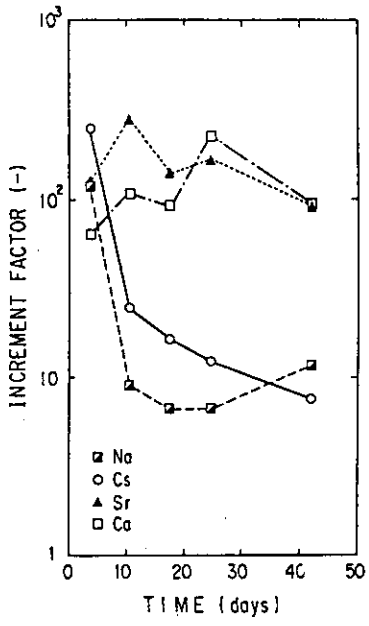

Fig. 10. Comparison of increments in normalized leach rates of indicator elements from curium-doped titanate ceramic after an equivalent age of 31000 yr. Increment factor is the ratio of the leach rate of each element from the 31000-yr samples to the analogous leach rate from the 130-yr samples.

Table IV. Chemical composition of the smectite.

composition	weight%
SiO_2	57.96
TiO_2	trace
Al_2O_3	21.87
Fe_2O_3	1.97
MnO	trace
CaO	0.54
Na_2O	2.98
K_2O	0.14
H_2O^+	5.71
H_2O^-	5.04
Total	99.6

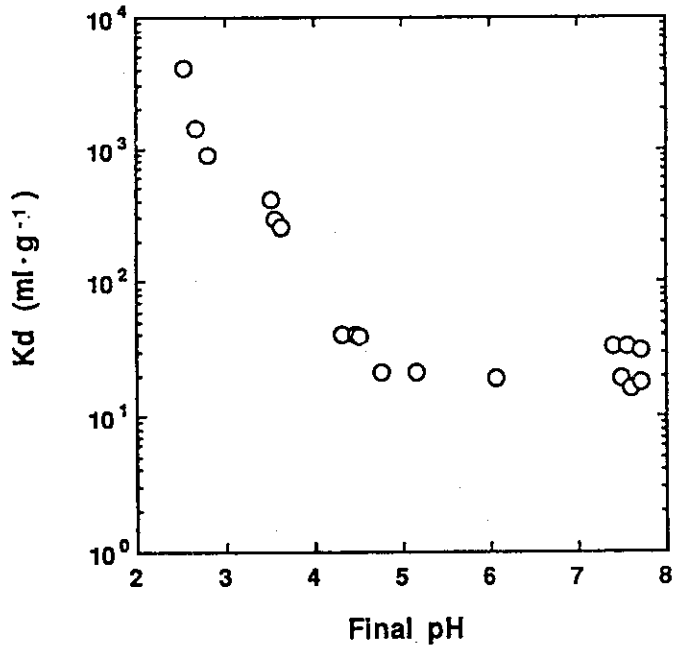

Fig.11. The pH dependence of Np distribution coefficient for smectite.

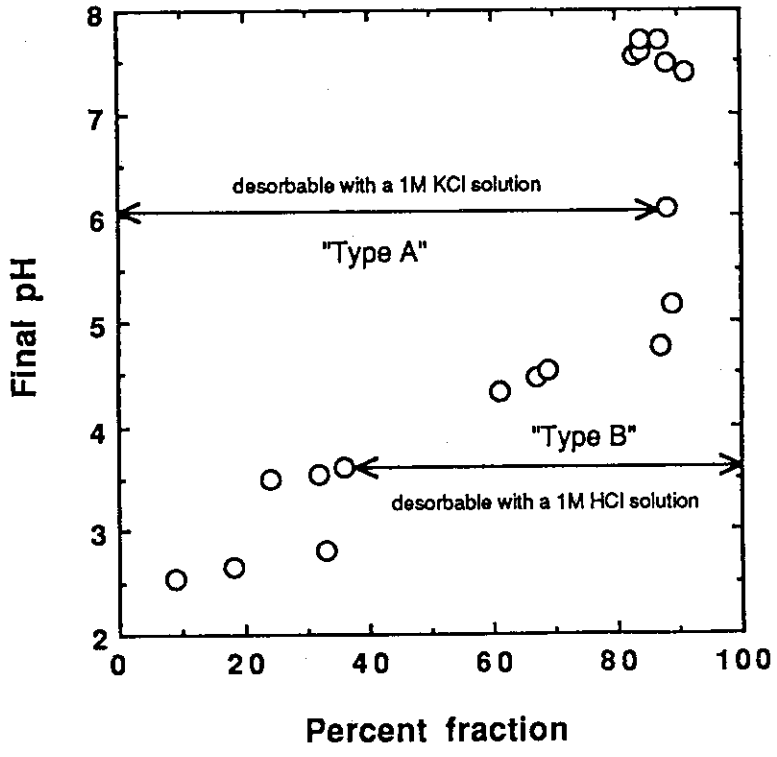

Fig.12. The pH dependence of Np fraction(%) desorbed by KCl and HCl solutions.

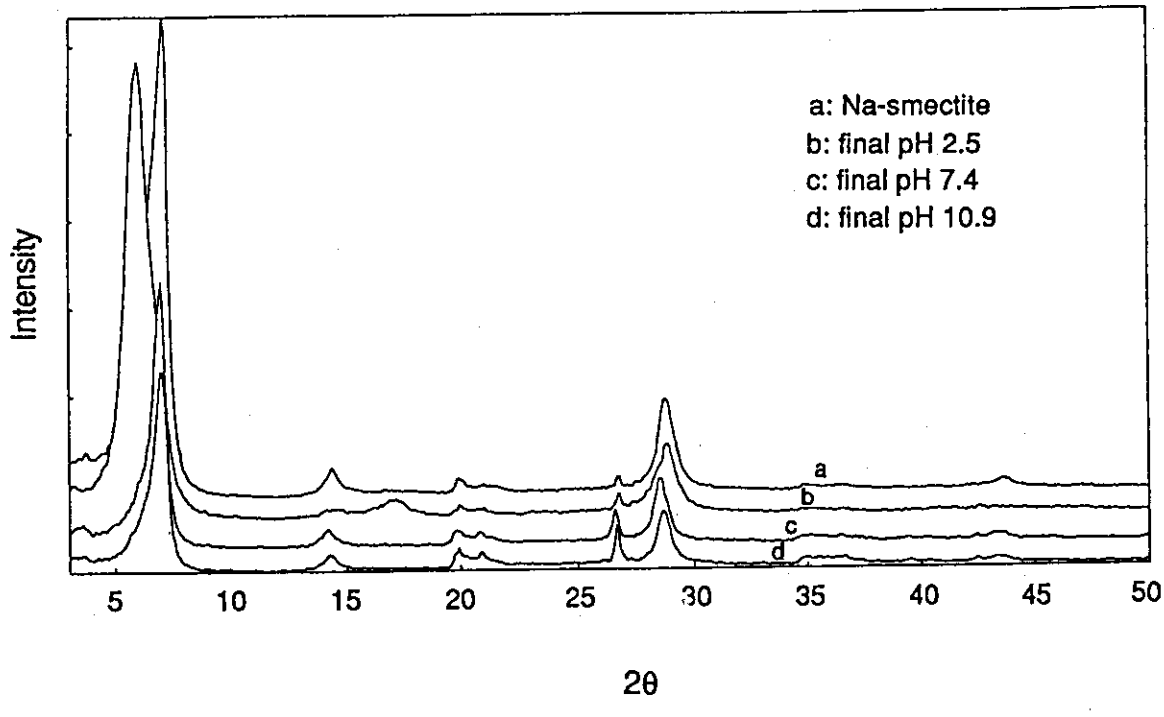

Fig.13. X-ray diffraction patterns of smectites after contacting with different pH solutions. The smectites used were dried after contacting with different pH solutions at 20°C for 10 days.